Formation, migration, and clustering of delocalized vacancies and interstitials at a solid-state semicoherent interface

Kedarnath Kolluri*

Department of Materials Science and Engineering, Massachusetts Institute of Technology, Cambridge, Massachusetts 02139, USA and MST-8, Materials Science in Radiation and Dynamic Extremes, Los Alamos National Lab, Los Alamos, New Mexico 87545, USA

Michael J. Demkowicz

Department of Materials Science and Engineering, Massachusetts Institute of Technology, Cambridge, Massachusetts 02139, USA

(Received 21 December 2011; published 10 May 2012)

Atomistic simulations are used to study the formation, migration, and clustering of delocalized vacancies and interstitials at a model fcc-bcc semicoherent interface formed by adjacent layers of Cu and Nb. These defects migrate between interfacial trapping sites through a multistep mechanism that may be described using dislocation mechanics. Similar mechanisms operate in the formation, migration, and dissociation of interfacial point defect clusters. Effective migration rates may be computed using the harmonic approximation of transition state theory with a temperature-dependent prefactor. Our results demonstrate that delocalized vacancies and interstitials at some interfaces may be viewed as genuine defects, albeit governed by mechanisms of higher complexity than conventional point defects in crystalline solids.

DOI: 10.1103/PhysRevB.85.205416 PACS number(s): 68.35.Fx, 61.72.J−, 66.30.−h

I. INTRODUCTION

Understanding the formation, motion, and clustering of vacancies and interstitials is indispensable for explaining numerous properties of crystalline solids. For example, migration of vacancies or interstitials is the mechanism of diffusion in most crystalline materials.[1] Formation of vacancies, interstitials, and clusters thereof is the primary form of radiation damage in polycrystals.[2] Their subsequent agglomeration and interaction with dislocations is responsible for multiple phenomena, such as dislocation creep,[3] void swelling,[4] and radiation-induced growth.[5]

Although much is known about vacancies and interstitials in perfect crystalline solids, a comparable understanding of those confined to internal interfaces [grain boundaries (GBs) and heterophase interfaces] is currently lacking. Such knowledge, however, is of increasing technological importance since interfaces often have a significant influence on the performance of miniaturized devices and on properties of nanostructured solids. In these cases, interactions of vacancies and interstitials with interfaces may be as important to a material's overall properties as point defects in the bulk. Some interfaces, such as coherent GBs, exhibit point defect behaviors not unlike those encountered in perfect crystals.[6–8] Point defects absorbed at some noncoherent interfaces, however, reconstruct into delocalized configurations that do not resemble conventional vacancies or interstitials.[9–13] The behavior of such configurations and their relation to properties such as diffusion are not intuitive.[14]

Our goal is to shed light on the behavior of defects that delocalize upon absorption at interfaces by determining if the formation, motion, and clustering of such delocalized configurations may be described through a limited set of atomic mechanisms ascribable to well-defined "defects." We focus our attention on a single model system, namely, a well-characterized heterophase interface found in magnetron sputtered Cu-Nb multilayer composites[13,15,16] and conclude that delocalized vacancies and interstitials at this interface do indeed form well-defined defects with definite atomic migration and clustering mechanisms. The complexity of these mechanisms is greater than that of conventional defects in crystalline materials, requiring different descriptions of defect reactions and modified expressions for migration rates. These mechanisms, however, may be related directly to the structure of the defect-free Cu-Nb interface, suggesting that some properties of delocalized interfacial point defects may be deduced from interface structure alone.

Early experimental studies of vacancies and interstitials at solid-state interfaces focused on self- and impurity diffusion. Paralleling contemporary understanding of diffusion in perfect crystals, most of these investigations proceeded on the hypothesis that mass transport occurred by a defect migration mechanism.[17,18] They found that interfaces generally exhibited greater self-diffusivities than the neighboring solids[19,20] and that self-diffusion at interfaces was usually anisotropic.[21] This finding was interpreted by relating interface diffusion to interface structure, which was modeled as a quasiperiodic array of coherent patches separated by highly distorted regions, the latter having elevated diffusivities.[22] In some cases, the distorted regions could simply be identified as misfit dislocations or disconnections,[23] while in others their identity was not as clear.[24]

This interpretation of interface diffusion in terms of interface structure agreed well with several studies of self- and impurity diffusion in GBs. For example, average diffusivities increased with increasing misorientation angle for tilt and twist GBs in fcc metals up to a critical angle.[21,25,26] Above that critical angle, diffusivities remained nearly misorientation independent. According to the misfit dislocation interface structure model, the density of dislocations at an interface increases with increasing misorientation between the grains. Therefore, the GB diffusivity increases and becomes more anisotropic at higher misorientations since the fast diffusion pathways are line defects with a definite spatial orientation.

Diffusion is easy in all directions when the spacing between fast diffusion pathways becomes sufficiently small, explaining the loss of misorientation dependence above a certain misorientation. Highly coherent GBs that correspond to "special" misorientations and GB plane orientations[6,7] do not contain any high diffusivity pathways and therefore exhibit self- and impuritiy diffusivities comparable to those in the adjoining crystals.

Experiments have therefore revealed clear connections between interface structure and diffusivity. In some cases, the associated atomic mechanisms of mass transport could also be deduced based on interface structure. For example, in coherent GBs, diffusion was thought to occur by the same vacancy diffusion mechanisms as in crystalline solids, an insight later confirmed by atomistic simulations.[8,27] In symmetric tilt GBs, diffusion was interpreted to occur by the same atomic mechanisms as those causing diffusion at dislocation cores in bulk materials.[28] Deduction of atomic mechanisms of mass transport in interfaces with more complex structures, however, has proven difficult. Direct experimental investigation of these mechanisms is not currently possible owing to the small length and time scales associated with them. Atomistic simulations, however, are well suited to such investigations.

Atomistic modeling investigations of GBs have found that interfacial point defects may be classified broadly into two categories based on their structure. Point defects absorbed at some GBs retain a compact structure, similar to that in perfect crystals.[12,14,29,30] In others, vacancies and interstitials delocalize by rearrangement of atoms further than the nearest neighbors.[9–12,14,30] In some cases, introduction of vacancies or interstitials may lead to extensive reconstruction of portions of the GB plane.[31,32] While the structure of compact point defects is well understood, that of delocalized ones is not.

Atomistic modeling has shown that interfacial point defect structures depend on interface structure and that they vary from location to location at individual interfaces: some interface sites may support compact point defects, whereas others allow only for delocalized ones.[13,33] There may also be sites that do not support any point defects at all. When introduced at such sites, vacancies and interstitials spontaneously move to other nearby sites that do support compact or delocalized point defects.[12–14] The generalizable insights from these studies are qualitative: coherent regions of interfaces typically support compact point defects, while delocalization is more likely at or near noncoherent ones.

Modeling has revealed that migration of point defects at interfaces may also be classified into two broad categories. In the first, compact point defects migrate between nearest-neighbor sites similarly to how they do in perfect crystals. In vacancy or interstitial exchange, only one atom is involved in the migration process,[34] while two atoms are involved in the interstitialcy mechanism.[18] In the second category, vacancies and interstitials migrate by collective motion of numerous atoms. Both compact[14,29,35,36] and delocalized point defects[12,33] may migrate in this manner. In the case of the former, collective migration likely occurs because the sites between the endpoints of the migration process do not support stable point defects.[12,14,33] Migration mechanisms of delocalized point defects, however, are generally not well understood.

By analogy with crystalline materials, where vacancies and interstitials aggregate into dislocation loops or voids, point defects at interfaces may also be expected to cluster. Nevertheless, direct investigations of this phenomenon are limited. King and Smith observed that vacancies trapped at coherent $\Sigma 3$ twin boundaries in Al and Cu form Frank dislocation loops, similar to what occurs in the corresponding single crystals.[37] Studies of helium bubble growth in GBs in austenitic steels and aluminum found that helium bubbles formed preferentially at the GBs containing misfit dislocation intersections and that these bubbles were always larger than in the crystal.[38,39] These observations suggest that vacancies may preferentially cluster at intersections of misfit dislocations. Detailed investigations of the atomic-level clustering mechanisms of delocalized vacancies and interstitials at interfaces, however, are not presently available.

In this paper, we present atomistic simulations that shed light on the structure, migration, and clustering of delocalized vacancies and interstitials in a model Cu-Nb heterophase interface.[13,15,16] In Sec. II, the construction of an atomic model of this interface and simulation methods used to study it are described. The structure of the defect-free interface and its behavior at finite temperature are described in Sec. III A and the structure of point defects and point defect clusters in it in Sec. III B. Simulations of migration of point defects (already presented in abbreviated form in Ref. 40) and point defect clusters are described in Sec. III C. In Sec. III D, a transition state theory-based kinetic model is presented to account for the multistep nature of the migration mechanism. Comparison of our conclusions with previous studies, implications for other interfaces, and limitations of our study are discussed in Sec. IV. Conclusions are presented in Sec. V.

II. INTERFACE MODEL AND SIMULATION METHODS

We conduct our investigation on an atomic model of an interface found in magnetron sputtered multilayer composites of face-centered-cubic (fcc) copper (Cu) and a body-centered-cubic (bcc) niobium (Nb). This interface forms with $\{111\}_{Cu}$ and $\{110\}_{Nb}$ terminal planes parallel to and abutting each other. Furthermore, $\langle 110\rangle_{Cu}$ and $\langle 111\rangle_{Nb}$ directions are parallel in the interface plane, so the neighboring Cu and Nb layers are in the Kurdjumov-Sachs orientation relation.[15] We create an atomic model of this interface by joining appropriately oriented Cu and Nb blocks as shown in Fig. 1(a). Each block is about 10 nm wide in the directions parallel to the interface plane and about 4 nm thick in the direction normal to the interface plane. The simulation supercell is periodic in the interface plane and terminates with free surfaces in the direction normal to the interface.

Interatomic interactions are modeled using an embedded atom method (EAM) potential. The EAM is a standard form for atomic interactions fitted to reproduce desired physical properties of solids.[41,42] The potential we used was constructed based on already available EAM descriptions of pure Cu and Nb. Cross-element interactions were fitted to reproduce the high positive dilute enthalpies of mixing of Cu in Nb and Nb in Cu as well as the lattice parameter and bulk modulus of a hypothetical Cu-Nb compound in the Cs-Cl structure.[43] This

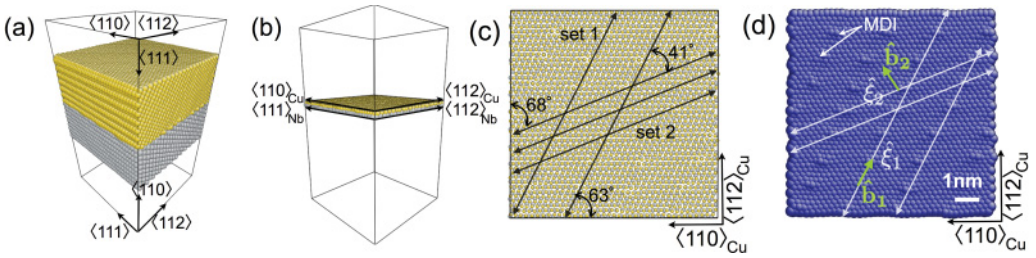

FIG. 1. (Color online) (a) Perspective view of the simulation cell showing Cu (gold) and Nb (gray) layers with free surfaces parallel to the interface. (b) Perspective view of the terminal Cu and Nb atomic planes. (c) Top-down view of the Cu and Nb terminal planes showing the locations of representative members of two parallel misfit dislocation arrays. Angles between the dislocations and x and y axes are labeled. (d) Cu terminal plane with representative misfit dislocations and corresponding Burgers vectors marked. Protrusions occur at intersections between misfit dislocations (MDIs).

potential has been used in numerous previous studies of the structure and properties of Cu-Nb interfaces.[13,16,40,44–46]

To relax the Cu-Nb interface, the neighboring Cu and Nb blocks were translated with respect to each other rigidly in both directions parallel to the interface. After each translation, the bilayer was relaxed by conjugate gradient potential energy minimization[47] (PEM) using LAMMPS.[48] The shape of the simulation cell was also relaxed,[48] yielding a zero average bilayer stress.[49] PEM was performed until the two-norm force on every atom in the simulation supercell was less than 0.1 pN. In agreement with previous studies,[50] the energy of this interface was found to be nearly independent of the rigid translations. The atomic configuration of the interface was stable in all our simulations up to $T = 900$ K and 8.11 ns.

Interface properties and point defect interactions with the interface were studied with canonical ensemble molecular dynamics (MD) simulations at constant volume using LAMMPS.[48] Temperatures were controlled using a Langevin thermostat.[51] Point defect behaviors, including the full migration path, were determined by direct inspection of the MD trajectories at the simulation temperature. PEM was only used for further analysis of metastable configurations identified in MD. Minimum energy paths (MEPs) between metastable configurations, including saddle-point configurations, were studied with the climbing image nudged elastic band (CINEB) method.[52,53] Calculations were considered to have converged when the maximum elastic-band force on every atom in every replica fell beneath 9 pN. Visualizations were performed using ATOMEYE.[54]

III. RESULTS AND ANALYSES

A. Structure of Cu-Nb interface

The Cu-Nb interface described in the previous section is semicoherent and contains two sets of closely spaced misfit dislocations that form a network spanning the entire interface, as shown in Figs. 1(c) and 1(d). Detailed analysis of these misfit dislocations is available in Ref. 16. Briefly, misfit dislocations in set 1 are spaced 2.17 nm apart, while those in set 2 are separated by 0.89 nm. The two sets of misfit dislocations make an angle of 41° between each other. The angles between the line vectors of sets 1 and 2 and their corresponding Burgers vectors are approximately 3° and 82°, respectively [Figs. 1(c) and 1(d)]. Hence, set 1 misfit dislocations are predominantly screw in character, while set 2 misfit dislocations are predominantly edge.

The potential energy landscape of the Cu-Nb interface contains multiple metastable minima separated by small energy barriers. This may be seen by quenching interface configurations saved periodically in a high-temperature ($T =$ 800 K) MD run. In an interface with just one minimum energy state, such as a coherent interface, each quenched configuration would have the same energy. In the Cu-Nb interface, however, variations in the energy of quenched configurations approaching 1 eV are found [Fig. 2(a)]. No changes in structure were detected at the free surfaces or in the crystalline layer during these simulations, so the observed energy variations may be attributed to the Cu-Nb interface.

This roughness of the interface potential energy landscape is due to fluctuations in atom positions at misfit dislocation intersections (MDIs), labeled in Fig. 1(d). While many fluctuations are small, some larger ones lead to nucleation of thermal kink pairs at MDIs [Fig. 2(b)]. The thermal kink pairs may be detected by finding clusters of four- and five-membered rings in the Cu terminal plane.[13,16] Burgers circuits enclosing the five-membered rings exhibit closure failures equal to the Burgers vector of set 1 misfit dislocation,[55] motivating the thermal kink model in Fig. 2(c).

The structural fluctuations occurring continually at the Cu-Nb interface at elevated temperatures give rise to energy variations that interfere with calculations of formation and

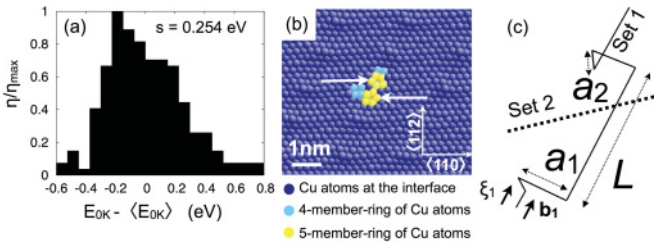

FIG. 2. (Color online) (a) Variations in energy upon multiple quenches from $T = 800$ K indicate that the Cu-Nb interface has a rough potential energy landscape. (b) Thermal kink pairs are one type of structural fluctuation that occurs at the Cu-Nb interface. Atoms colored yellow form five-membered rings in the terminal Cu plane and correspond to the locations of kinks on misfit dislocations. Arrows indicate atomic half-planes that terminate at these kinks. (c) A dislocation model for the thermal kink pair in (b).

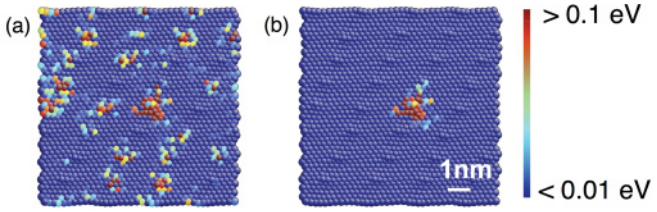

FIG. 3. (Color online) Differences in atomic energy in the Cu terminal plane between an interface containing a thermal kink pair at the center and the reference configuration in Fig. 1(d). (a) Direct comparison of an interface structure obtained from MD and (b) of one where atomic positions outside a test region containing the kink pair were restored to their positions in the reference configuration.

migration energies of thermal kink pairs and other defects. Figure 3(a) plots differences in atomic energies in the Cu terminal plane between an interface with a single thermal kink pair and a reference configuration [the interface in Fig. 1(d)]. Marked changes in energy due to independent structural fluctuations may be seen far from the kink pair, which is located at the center of the figure. Thus, defect energies may not be calculated by directly comparing quenched configurations to a single reference interface structure.

To filter out the effect of uncorrelated structural fluctuations, we identified a test region surrounding the defect of interest, in this case the thermal kink pair. Atomic positions outside that region were substituted with those obtained from the reference configuration. Only the atomic positions inside the test region were left unchanged. The resulting interface structure was then relaxed using PEM and atomic energy changes were computed between it and the reference configuration. Figure 3(b) shows that, for a sufficiently small test region, energy changes due to distant structural fluctuations could be removed. Test regions were chosen to be as small as possible so long as the defect of interest remained stable.

Using this approach, the formation energies of thermal kink pairs $\Delta E^{\text{form}}_{\text{kink pair}}$ were found to lie between 0.27 and 0.35 eV. Activation energies for thermal kink pair nucleation were determined using the CINEB method with initial chains of states constructed by linear interpolation between the reference state, where no thermal kink pair exists, and the configuration with the thermal kink pair after removing the structural fluctuations. The activation barrier was found to be $\Delta E^{\text{act}}_{\text{kink pair}} \approx 0.45$ eV.

B. Isolated and clustered vacancies and interstitials at the Cu-Nb interface

A detailed discussion of isolated point defects including their structural features is available in Refs. 13 and 16. Briefly, both vacancies and interstitials bind to the Cu-Nb interface, albeit more strongly in the Cu terminal plane than in the Nb terminal plane. Vacancy and interstitial binding energies in the former are as high as ∼1.6 and ∼2.7 eV, respectively,[16] where binding energy is defined as the energy released after a point defect is moved from a perfect crystal to the interface. At certain locations in the interface, the difference in defect formation energies between terminal Cu and Nb planes is larger than the energy penalty associated with atomic mixing, causing defects in the Nb terminal plane to move spontaneously into the Cu terminal plane, where they

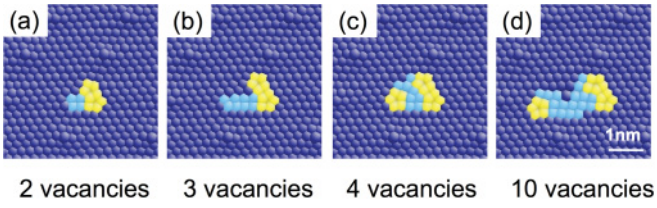

FIG. 4. (Color online) Clusters of vacancies form kink-jog combinations at MDIs. Atom coloring is the same as in Fig. 2(b).

may undergo further migration and clustering. Therefore, we restrict our investigation to point defects at Cu terminal plane. Vacancies are introduced by removing Cu atoms, whereas interstitials are introduced by adding Cu atoms.

Point defects in fcc Cu have conventional, compact structures.[16] By contrast, regardless of where they are introduced in the Cu terminal plane, isolated vacancies and self-interstitials in the Cu terminal plane of the Cu-Nb interface migrate to MDIs, where they delocalize into kink-jog pairs, as illustrated in Fig. 7(a) for a vacancy and Fig. 7(g) for an interstitial, and are trapped at those MDIs. These delocalized point defects may be detected by finding atoms that form four- and five-membered rings, as was done for the thermal kink pair in Sec. III A. Their structure may be modeled as illustrated in Figs. 7(d) and 7(j), which show that delocalized vacancies and self-interstitials cause a set 1 misfit dislocation to climb by one atomic plane into the neighboring fcc Cu layer, allowing it to avoid intersecting with a set 2 misfit dislocation in the Cu-Nb interface.

Vacancy and interstitial clusters were created by removing or adding multiple Cu atoms at the same MDI. The resulting structures were relaxed using PEM and then annealed at $T = 800$ K for 0.8 ns. Only clusters containing up to 10 vacancies and 5 interstitials were investigated in this study, as larger ones dissociated into multiple clusters occupying several neighboring MDIs. Representative point defect cluster configurations are shown in Figs. 4 and 5. Similar to isolated point defects, point defect clusters delocalize into kink-jog configurations on interface misfit dislocations that may be detected by finding four- and five-member rings. Unlike isolated delocalized vacancies, which reside on set 1 misfit dislocations, vacancy clusters tend to extend along set 2 misfit dislocations, as shown in Fig. 4(d). Interstitial clusters, however, extend exclusively along set 1 misfit dislocations [Fig. 5].

Formation energies of point defect clusters at MDIs were computed as $\Delta E = E_{\text{cluster}} - (E_0 + \Delta N E_{\text{coh}})$ and are shown in Fig. 6. E_{cluster} is the energy of the system containing the

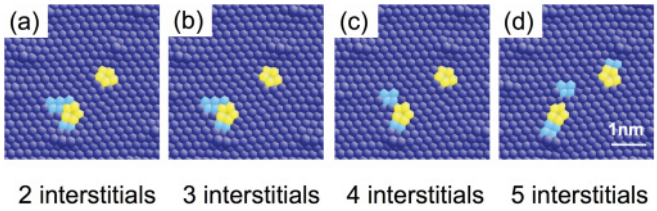

FIG. 5. (Color online) Similar to isolated self-interstitials [Fig. 7(g)], clusters of interstitials form kink-jog pairs at MDIs. Atom coloring is the same as in Fig. 2(b).

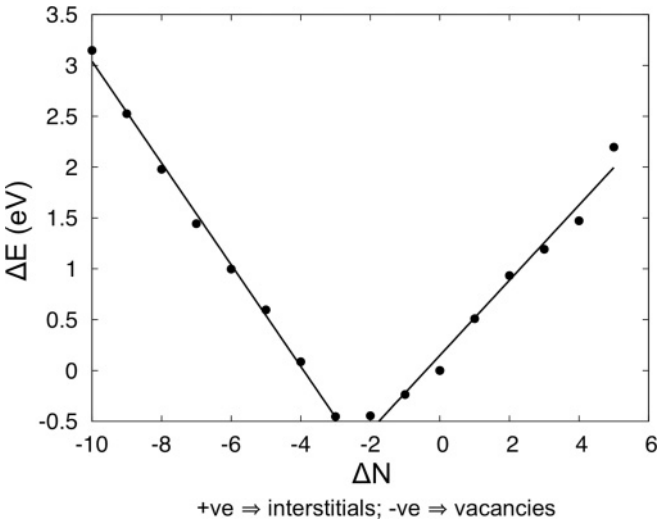

FIG. 6. Formation energies of point defect clusters at an MDI in the Cu-Nb interface. The x axis shows the number of point defects created in a defect-free interface, such as that shown in Fig. 1(d). The lines are best fits to the vacancy and interstitial formation energies relative to the ground-state interface ($\Delta N = -2$ or -3).

point defect cluster and $E_{\rm coh} = -3.54$ eV is the cohesive energy of Cu for the potential used in this study.[43] ΔN is the number of point defects in the cluster, where $\Delta N < 0$ for vacancy clusters and $\Delta N > 0$ for interstitial clusters. E_0 is the energy of a reference state. Here, we choose the interface, like that in Fig. 1, with no point defects ($\Delta N = 0$) as the reference state. ΔE is negative for $\Delta N \in \{-1, -2, -3\}$, i.e., for clusters containing between one and three vacancies, and reaches a minimum for $\Delta N \in \{-2, -3\}$. Because clusters containing up to three vacancies are tightly confined to just one single MDI, we find the interaction energies between vacancy clusters at adjacent MDIs to be negligible. Therefore, in agreement with previous studies,[13,16,56] the Cu-Nb interface in its ground state must contain two or three vacancies at each MDI.

Defect cluster energies ΔE increase approximately linearly with departures of ΔN from the ground state. This linear dependence implies that vacancies or interstitials added to the interface in its ground state are equally likely to remain isolated as they are to form clusters. This behavior stands in stark contrast to vacancy and interstitial clustering in crystalline Cu, where the energy of a cluster of vacancies/interstitials is always lower than the sum of the energies of equal numbers of isolated point defects,[57–59] providing a thermodynamic driving force for clustering. By contrast, there is no such driving force in the Cu-Nb interface. Thus, since the configurational entropy of point defect clusters is lower than the entropy of an equal number of isolated point defects at nonzero temperature, point defects in Cu-Nb interfaces are likely to evaporate from clusters and remain isolated thereafter.

Indeed, vacancy clusters containing between 7 and 10 vacancies ($-10 \leqslant \Delta N < -6$) breakup within 80 ps at temperatures as low as 500 K. Moreover, vacancy clusters containing more than 10 vacancies ($\Delta N < -10$) spontaneously dissociate into separate clusters residing at neighboring MDIs. Interstitial clusters containing more than 5 interstitials ($\Delta N > 5$) extend to reside on multiple MDIs and often break up into smaller clusters when annealed at 800 K for about 1 ns. These smaller clusters are separated by at least one defect-free MDI because interstitial clusters residing on adjacent MDIs are large enough to overlap.

C. Vacancy and interstitial migration and clustering at the Cu-Nb interface

Migration and clustering mechanisms of point defects (isolated as well as clusters) were identified directly in $T = 800$ K MD simulations. Atomic configurations from MD simulations were saved and analyzed at frequent intervals, some as small as 0.811 fs, but none longer than 20.28 ps. Whenever a change in defect structure or location was observed, these configurations were quenched using PEM to identify metastable states. Only those quenched configurations that closely resembled the defect state in the corresponding high-temperature configuration were considered to be metastable states. The resemblance was determined based on identification of fourfold and fivefold atomic rings in the Cu terminal plane.

1. Migration of individual vacancies and interstitials

Individual delocalized vacancies and interstitials migrate between neighboring trapping sites, i.e., from one MDI to another. Their motion is one-dimensional and proceeds along set 1 misfit dislocations through a two-stage process. First, a defect delocalized at one MDI extends to reside on two MDIs [Figs. 7(b) and 7(h)]. Next, it collapses back onto a neighboring MDI [Figs. 7(c) and 7(i)], completing the migration process. The energy difference between the collapsed state, termed A, and the extended one, B, was found to be in the range $\Delta E_{A\to B} = 0.06{-}0.12$ eV.

Transitions between each state are thermally activated and involve the nucleation of metastable thermal kink pairs, similar to the one discussed in Sec. III A and shown in Fig. 2(b). First, a thermal kink pair, comprised of two kink-jog combinations labeled $KJ3$ and $KJ4$ in Fig. 8(a), nucleates at an MDI adjacent to the delocalized vacancy, which consists of kink-jogs labeled $KJ1$ and $KJ2$. Next, one of the kink-jogs of the delocalized vacancy interacts to annihilate with the closest kink-jog of the thermal kink pair. Afterward, only kink-jogs $KJ1$ and $KJ4$ remain, corresponding to the extended state B shown in Figs. 7(b) and 7(h).

The transition from the extended state B in Fig. 7(b) [Fig. 7(h)] to the collapsed state A in Fig. 7(c) [Fig. 7(i)] is also mediated by a thermal kink pair. Figure 8(b) shows a configuration where the indicated kink pair $KJ2'{-}KJ3'$ forms between the two MDIs on which the point defect $KJ1{-}KJ4$ is delocalized. The kink-jogs $KJ1$ and $KJ2'$ together are equivalent to the thermal kink pair in Fig. 2(b) and the entire structure is equivalent to that in Fig. 8(a). Therefore, these kink-jogs may interact to annihilate. When they do, the defect has completed its migration to an adjacent MDI. The states in Figs. 8(a) and 8(b) are both termed I as they are energetically equivalent. The formation energy of a thermal kink pair in an I-type state is $\Delta E_{A\to I} = 0.25{-}0.35$ eV, the same as for the isolated thermal kink pair in Fig. 2(b).

The geometric configurations of the kink-jogs determine whether a given kink-jog pair will annihilate. For example, thermal kink pairs between the kink-jogs in extended defect

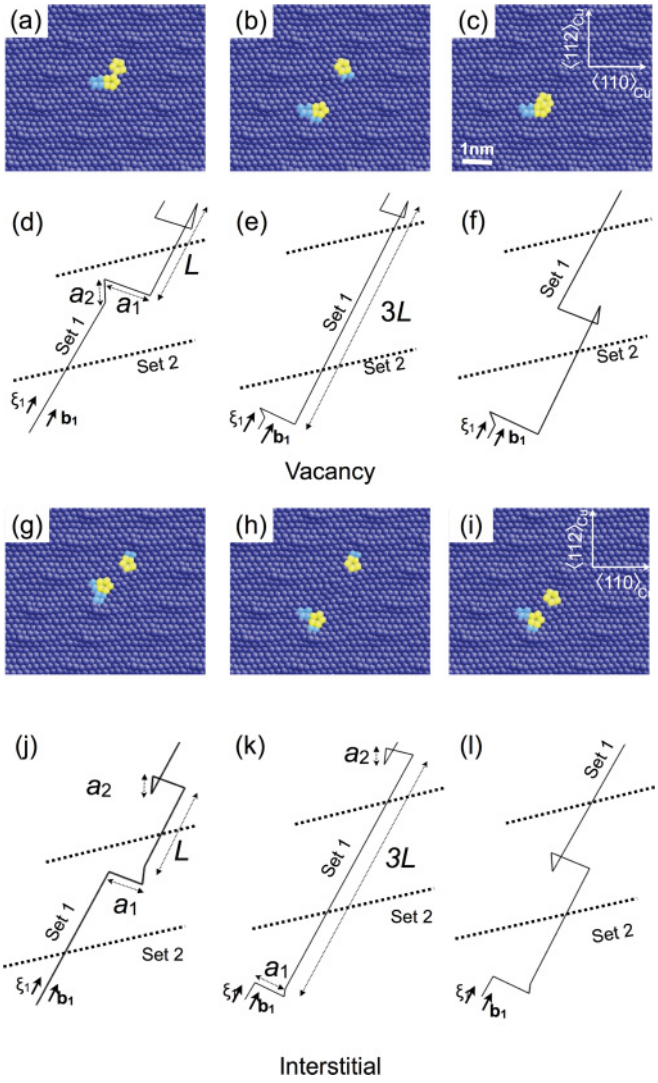

FIG. 7. (Color online) Migration of a delocalized vacancy (interstitial) from one MDI (a) [(g)] to another (c) [(i)] through the intermediate state (b) [(h)]. Atom coloring is the same as in Fig. 2(b). Dislocation models for configurations (a)–(c) are depicted (d)–(f) and those for (g)–(i) are depicted in (j)–(l).

state B were observed in a variety of different configurations in our simulations. One such configuration, shown in Fig. 8(c), differs from those in Figs. 8(a) and 8(b) because the number of ⟨110⟩-oriented lines of atoms between the five-member rings of the marked thermal kink pair in Fig. 8(c) is one less than that between the corresponding ones in Figs. 8(a) and 8(b). This difference may be due to fewer dislocation segments in the thermal kink pair in Fig. 8(c) than those in Figs. 8(a) and 8(b) and is illustrated in the dislocation models in Figs. 8(d) and 8(f). Because of these differences, kinks $KJ2''$ or $KJ3''$ in Fig. 8(c) can annihilate neither $KJ1$ nor $KJ4$. Such thermal kink pairs therefore do not participate in point defect migration. They may increase the residence time of the defect in the extended state by reducing the effective migration attempt frequency, thereby reducing the overall migration rate. The activation barrier for the nucleation of such thermal kink pairs is about 0.2 eV, i.e. smaller than that of regular ones.

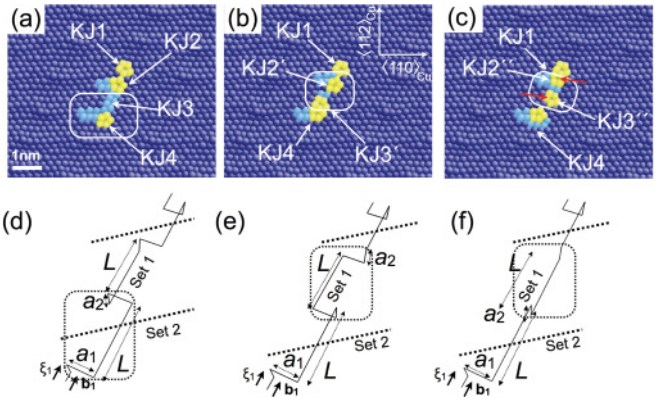

FIG. 8. (Color online) Thermal kink pairs nucleated at (a) an MDI adjacent to that of a vacancy and (b), (c) between the kink-jogs of a vacancy extended over two MDIs. Dislocation models for configurations (a)–(c) are depicted in (d)–(f), respectively. Red arrows in (c) mark the locations of kink-jogs in the indicated kink-jog pair, showing that they are separated by fewer ⟨110⟩ planes than those in (a) and (b). Atom coloring is the same as in Fig. 2(b).

The activation barriers for each step in point defect migration were determined by using the CINEB method on successive metastable states. Figure 9 shows several representative MEPs of individual delocalized point defects. States **A**, **B**, and **C**, correspond to configurations in Figs. 7(a)–7(c) for a vacancy [Figs. 7(g)–7(i) for an interstitial], respectively. The intermediate states **I** correspond to those in Figs. 8(a) and 8(b), while **I′** is the state in Fig. 8(c). The black curve in Fig. 9 shows the migration path of a delocalized vacancy that visits every possible metastable state. The complete path may be summarized as $\mathbf{A} \rightarrow \mathbf{t} \rightarrow \mathbf{I} \rightarrow \mathbf{t} \rightarrow \mathbf{B} \rightarrow \mathbf{t} \rightarrow \mathbf{I} \rightarrow \mathbf{t} \rightarrow \mathbf{C}$, where **t** represents saddle-point configurations.

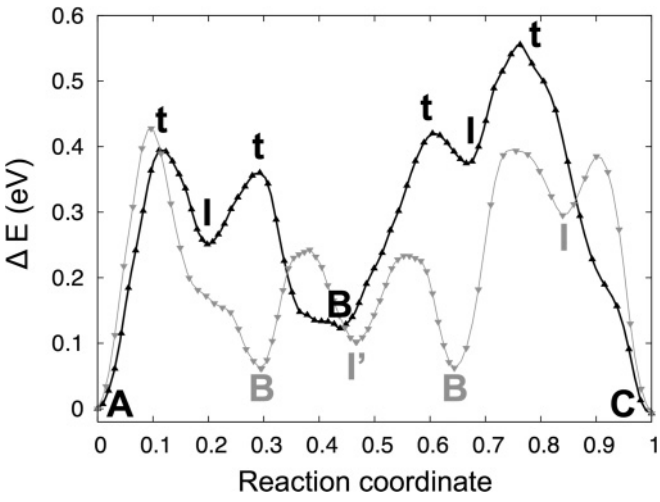

FIG. 9. Examples of different MEPs for isolated vacancy migration. **A**, **B**, and **C** correspond to the states shown in Figs. 7(a)–7(c), respectively. [In MEPs of interstitials, which have similar qualitative features (see Fig. 4 of Ref. 40 for an example), they correspond to Figs. 7(g)–7(i), respectively.] **I** corresponds to thermal kink pairs that aid defect migration, as in Figs. 8(a) and 8(b). **I′** is a kink pair that does not aid migration, as in Fig. 8(c). Examples of transition states **t** are shown in Fig. 10.

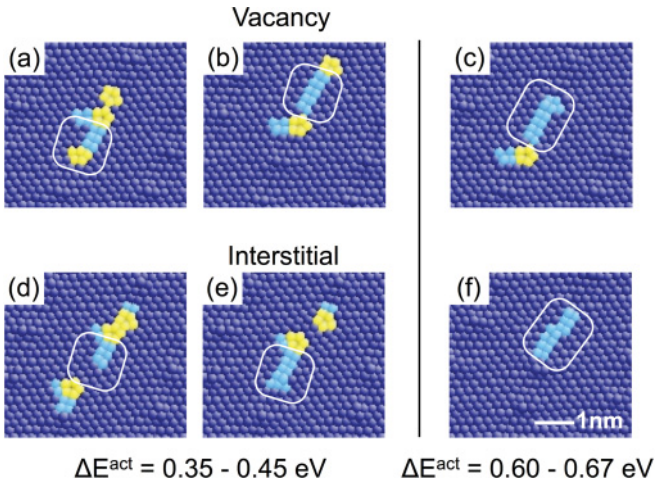

FIG. 10. (Color online) Examples of saddle-point configurations encountered during the migration of (a)–(c) a vacancy and (d)–(f) an interstitial. The activation barrier increases with the size of the region that has been sheared to create thermal kinks (represented by the four-member rings marked with white contours). Atom coloring is the same as in Fig. 2(b).

Representative saddle-point configurations are shown in Fig. 10. The activation barriers in the migration path correspond to nucleation or annihilation of thermal kinks. Hence, the energy along the path corresponds to the energy required to shear adjacent close-packed planes with respect to the other, known as the Peierls energy,[55] and depends on the area of the sheared region. For typical shearing areas observed in our simulations, the activation energies were in the range $E^{\mathrm{act}} = 0.35$–0.45eV. These shearing regions were observed when two of the kink-jogs are delocalized as seen in the left panel of Fig. 10. Occasionally, the shearing areas are larger, as in the right panel of Fig. 10. The corresponding activation barriers were higher: $E^{\mathrm{act}} = 0.60$–0.70 eV.

Delocalized point defects can migrate through several different MEPs. The gray curve in Fig. 9 shows a MEP for a migrating vacancy in which a thermal kink pair $\mathbf{I}'$ that does not aid migration [similar to that shown in Fig. 8(c)] nucleates and vanishes. It is also possible for a migrating point defect not to visit all metastable states available along the MEP. For example, a vacancy or interstitial may traverse a path that begins with the sequence $\mathbf{A} \rightarrow \mathbf{t} \rightarrow \mathbf{B}$ (gray curve), which does not include the state **I**, instead of the complete one $\mathbf{A} \rightarrow \mathbf{t} \rightarrow \mathbf{I} \rightarrow \mathbf{t} \rightarrow \mathbf{B}$ (black curve). In such MEPs, incipient thermal kink pairs interact with kink-jog segments of the delocalized point defect even before the former fully nucleate, thereby bypassing the metastable state **I**.

Thus, delocalized point defects at Cu-Nb interfaces may migrate through many different MEPs. Nevertheless, transitions between **A**, **B**, and **C** states in every path occur through the formation, interaction, and annihilation of kink-jogs. Furthermore, the path between any two of these states proceeds through a limited number of saddle-point types, the structure and energy of which depends on the adjacent metastable states. It may be possible to enumerate the structures and energies of all of these saddle points because they differ only in their number of delocalized kink-jogs and the extent of their delocalization. Any given migration path samples from this ensemble of possible transition states.

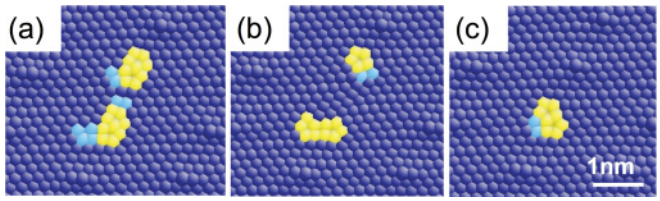

FIG. 11. (Color online) Clustering of two vacancies delocalized at adjacent MDIs (a) into a divacancy (c). The clustering mechanism is similar to that for migration of isolated point defects. In an intermediate state (b), the divacancy resides on two MDIs. Atom coloring is the same as in Fig. 2(b).

2. *Formation, migration, and dissociation of vacancy and interstitial clusters*

Similar to migration of isolated point defects, the kinetics of point defect cluster formation, migration, and dissociation were studied by direct observation of transitions occurring in MD. Individual vacancies introduced at adjacent MDIs in the defect-free interface shown in Fig. 1(d) were observed to coalesce into an energetically favorable divacancy (Fig. 11). The coalescence mechanism is similar to the migration mechanism of individual point defects. First, two kink-jogs, one from each delocalized vacancy, interact to annihilate each other forming a defect cluster (divacancy) residing on two MDIs. Next, thermal kink pairs nucleate between the kink-jogs of the divacancy and annihilate one of the jogs to complete the coalescence of the vacancies (Fig. 11). As shown in Sec. III B, divacancies have a lower formation energy than isolated vacancies in the defect-free interface and are therefore more stable.

Divacancies may migrate from one MDI to another without dissociating, as shown in Fig. 12. The migration mechanism is similar to that of an individual vacancy with an intermediate extended state [Fig. 12(b)]. Transitions between successive states in divacancy migration are aided by thermal kink pairs forming either at adjacent MDIs or between the kink-jogs of the extended defect. Clusters containing more than two vacancies dissociate into smaller clusters before migrating. For example, the trivacancy shown in Fig. 13(a) dissociates into a divacancy and a single vacancy [Fig. 13(c)]. Dissociation of the trivacancy also occurs by a multistage process with

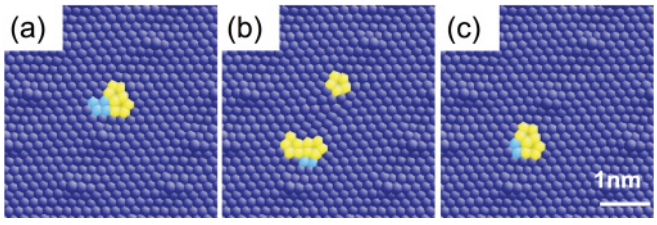

FIG. 12. (Color online) The migration mechanism of a divacancy is similar to that of a single vacancy. In the intermediate state (b), the divacancy extends to reside on two MDIs. Atom coloring is the same as in Fig. 2(b).

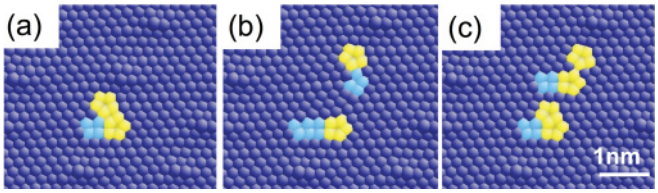

FIG. 13. (Color online) Dissociation of a trivacancy (a) into a divacancy and a monovacancy (c) is aided by the formation, migration, and annihilation of kink-jogs. In the intermediate state, the trivacancy resides on two MDIs. Atom coloring is the same as in Fig. 2(b).

an extended intermediate state and transitions between states aided by thermal kink pairs [Fig. 13(b)].

Similar to vacancy clusters, interstitial clusters migrate between neighboring MDIs through a multistage process with transitions aided by thermal kink pairs. These clusters also have intermediate states extended over two MDIs. Examples of migration of two-interstitial and three-interstitial clusters are shown in Fig. 14. The activation energy barriers for the clustering, migration, and dissociation processes described above were determined by the CINEB method. In all cases, activation energies for these processes were in the same range as those for isolated vacancies and interstitials.

3. *Why does point defect migration involve thermal kink pair formation?*

The point defect formation, migration, and clustering mechanisms described above may be modeled using dislocation mechanics. In fact, complete MEPs for point defect migration may be calculated analytically using these models. The detailed calculations required are given in Ref. 40, Eqs. (1)–(3). These equations account for the self-energy of each dislocation segment as well as the interaction energies of all pairs of segments along the set 1 misfit dislocation along which migration occurs. A single fitted constant must be specified to fully parametrize the model, namely, the dislocation core radius α.[55] We obtained α by fitting the formation energy of a thermal kink pair in the absence of delocalized point defects.[40] Despite the many approximations made in constructing this model, the MEPs it predicts are in remarkable quantitative agreement with those computed using the CINEB in the fully atomistic simulations (see Ref. 40 for details).

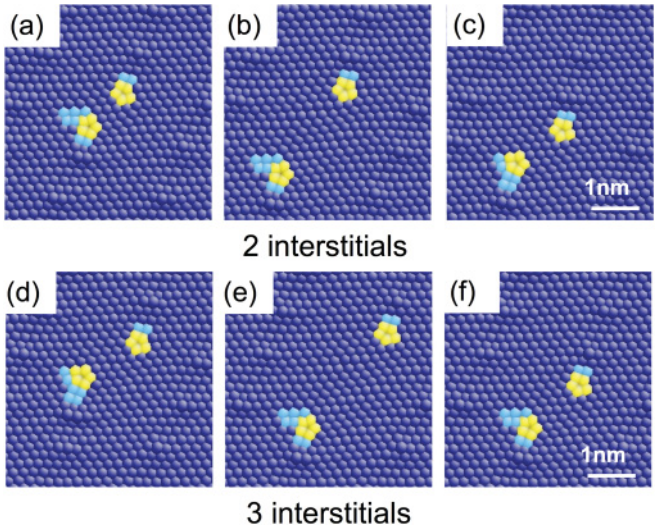

FIG. 14. (Color online) Migration of interstitial clusters occurs through an extended intermediate state where the clusters reside on two MDIs. Atom coloring is the same as in Fig. 2(b).

In view of the success of this dislocation-based model, however, it is not immediately clear why point defect migration is always accompanied by formation of thermal kink pairs. According to this model, the change in energy of a delocalized point defect as a function of separation x between its constituent kink-jogs, with respect to that of a point defect delocalized at a single MDI whose constituent kink-jogs are separated by L, is $W(x) - W(L)$, with $W(x)$ given by

$$W(x) = 2\frac{\mu b^2}{4\pi}\left[\sqrt{x^2+k^2} - x - k + x\ln\left(\frac{2x}{\sqrt{x^2+k^2}+x}\right)\right] \times \sum_{i,j\in\{1,2\};i\neq j} -\frac{\mu b^2}{4\pi(1-\nu)} \times \left[2x_i - 2\sqrt{x_i^2+a_j^2} - 2a_j\ln\left(\frac{x_i}{\sqrt{x_i^2+a_j^2}+a_j}\right)\right], \quad (1)$$

where $k = \sqrt{a_1^2+a_2^2}$ and $x_i = \sqrt{x^2+a_i^2}$ (see dislocation models in Figs. 7 and 8). We obtain from MD simulations $a_1 = \frac{a_{Cu}}{\sqrt{3}}, a_2 = \frac{a_{Cu}}{\sqrt{2}}$, and $L = \frac{3a_{Cu}}{\sqrt{2}}$, where $a_{Cu} = 3.615$ Å, and $L \leqslant x \leqslant 3L$. For Cu at T = 0 K, $\mu = 43.6$ GPa and $\nu = 0.361$.[60] In addition, we take $b = \frac{a_{Cu}}{\sqrt{2}}$ from Ref. 16. Thus, the energy of a delocalized point defect should increase monotonically (without an energy barrier) from 0 to $\approx$0.13 eV if one of the kink-jogs in Fig. 8(a) were to simply migrate one neighbor at a time to an adjacent MDI without the aid of thermal kinks. The MEP computed for such a hypothetical direct migration mechanism using Eq. (1) is shown as a continuous curve in Fig. 15(a). If this mechanism could indeed operate, then it would have to be the dominant one since the barrier for thermal kink pair nucleation is about 0.4 eV. In fact, however, the direct migration mechanism is never observed in the simulations. This fact cannot be explained by lattice resistance since a kink-jog migrating one atomic nearest-neighbor distance at a time shears a relatively small area and therefore incurs a small migration barrier: on the order of of 10^{-3}eV.[61,62]

To understand why the direct migration mechanism does not occur, we constructed atomic configurations where one of the kink-jogs was artificially displaced by increments of one atomic nearest-neighbor distance. The extended state **B** is reached upon six such displacements, so the location of the kink-jog may be expressed using an integer parameter S, where $S = 0$ and $S = 6$ correspond to **A** and **B**, respectively, and $\frac{a_{fcc}}{\sqrt{2}}S$ is the displacement of the kink-jog for any value of S. Changes in defect energies with respect to $S = 0$ of each of the constructed configurations are plotted as filled squares in Fig. 15. The energy barrier for direct migration is found to be $\Delta E^{act} \approx 1.35$ eV, three times higher than for the thermal kink pair-mediated migration mechanism and an order of magnitude greater than that predicted by the dislocation model.

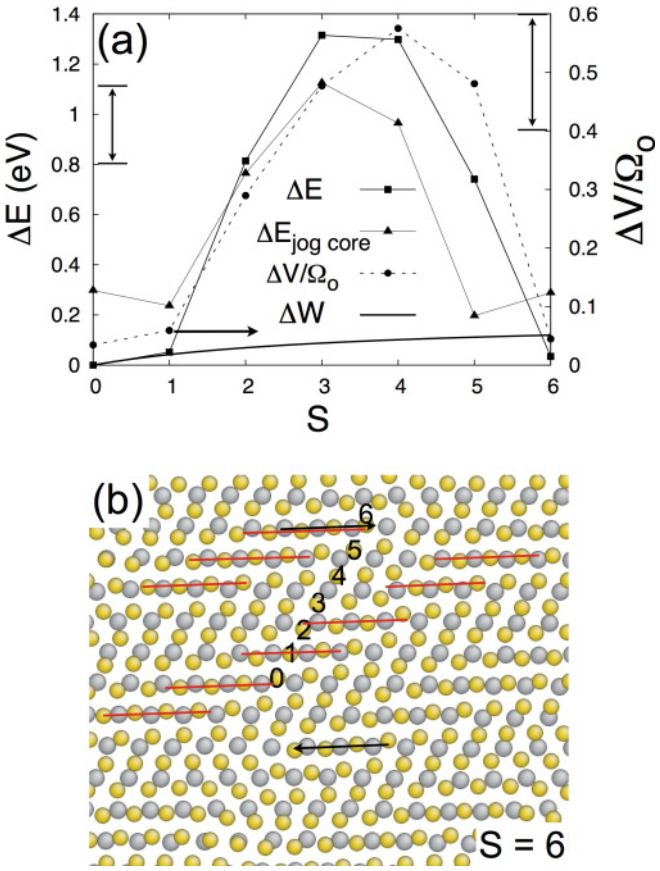

FIG. 15. (Color online) (a) Total energy change (filled squares), kink-jog core energy (filled triangles), and the energy from the dislocation model (continuous curve) for the direct migration mechanism. Filled circles show the kink-jog core volume. The arrow on the left shows the range of formation energies computed for a $\frac{a_{Cu}}{4}\langle 112\rangle$ jog on a screw dislocation in fcc Cu and the arrow on the right shows the corresponding formation volumes. (b) Plan view of the interface Cu (gold) and Nb (gray) atoms with a point defect in extended state **B**. Arrows mark the location of kink-jogs, the numbers are values of S, and red lines mark the nominal locations of set 2 misfit dislocation cores.

The above discrepancy arises because the core energy of the jog, which is assumed constant for all states in our dislocation model [and therefore does not appear in Eq. (1)], actually varies along the direct migration path. To estimate the core energy of the kink-jog, we summed differences in atomic energies between the core atoms and corresponding atoms in a defect-free interface. The kink-jog core is taken to consist of 19 atoms: the 5-atom ring in the Cu terminal plane and the 7 neighboring Cu and Nb atoms from each of the two planes adjacent to the Cu terminal plane. Core volumes were computed in an analogous way. The core energies of the migrating jog are plotted as filled triangles in Fig. 15(a) and are in good semiquantitative agreement with the overall energy changes occurring along the direct migration path. Core volumes are plotted as filled circles.

Figure 15(b) shows the Cu and Nb interface planes with a point defect in the extended state **B**. Arrows mark the locations of the two kink-jogs and red lines mark the nominal locations of set 2 misfit dislocation cores. The numbers are values of the displacement parameter S. At all values of S except $S \in \{3,4\}$, the kink-jog resides in the vicinity of a set 2 misfit dislocation, which affects its structure. The atomic configurations of the kink-jog at $S \in \{3,4\}$ were compared to that of a constricted $l = \frac{a_{Cu}}{4}\langle 112\rangle$ jog on a screw dislocation in fcc Cu.[61,62] Depending on the choice of reference energies and volumes, the core energy and volume of the $l = \frac{a_{Cu}}{4}\langle 112\rangle$ jog were found to be $\sim 0.8-1.1$ eV and $\sim 0.4\Omega_o - 0.6\Omega_o$, respectively, where $\Omega_o = 13.339$ Å^3 is the atomic volume of fcc Cu. These values compare very well with those obtained for the jog at $S \in \{3,4\}$, which are also the states where the kink-jog core energy is largest.

Thus, the true energy barrier for the direct migration mechanism is roughly equal to the difference in the formation energies of the jog at the MDI and that of an isolated jog on a screw dislocation. The dislocation model may be modified to account for such a behavior by allowing the core radius α to change with the distance between the jogs (S). Although irrelevant in the Cu-Nb interface, the direct migration mechanism may occur in other interfaces where the activation energy for thermal-kink-pair nucleation is comparable to the difference in kink-jog core energies described above. Furthermore, we expect that the direct migration mechanism, when active, would be highly pressure sensitive on account of its high activation volume.

D. Temperature dependence of point defect migration

As described in Sec. III C, delocalized interface point defects jump between MDIs through multiple steps. Kinetic Monte Carlo (kMC) simulations[63] may be used to determine the temperature dependence of the effective migration rate due to these numerous transitions. Since the vacancy and interstitial migration is along set 1 misfit dislocations, we consider migration only in one dimension. The transitions we take into account along with their activation energies are listed in Table I. In each transition listed in Table I, the start and end states are connected through just one path, but there may be more than one end state accessible for a given starting state. For example, a defect at its initial state **A** has two **I** states,

TABLE I. Transitions occurring during migration of individual point defects that were considered in kMC simulations, their corresponding activation energy barriers, and number of distinct end states for a given start state.

Transition type	Activation energy (eV)	Number of distinct end states
$A \rightarrow I$	0.40	2
$A \rightarrow B$	0.40	2
$I(\text{near } A) \rightarrow B$	0.15	1
$I(\text{near } A) \rightarrow A$	0.15	1
$B \rightarrow A$	0.35	1
$B \rightarrow I$	0.35	2
$B \rightarrow I'$	0.20	1
$B \rightarrow C$	0.35	1
$I(\text{near } C) \rightarrow C$	0.15	1
$I(\text{near } C) \rightarrow B$	0.15	1
$I' \rightarrow B$	0.15	1

one in the negative direction and the other in the positive direction. The number of distinct end states is also listed in Table I. The rates of individual transitions are determined using the harmonic approximation of transition state theory (TST) due to Vineyard[64] where the frequency of each transition is given by $\Gamma = \nu_0 e^{-\frac{E^{act}}{k_B T}}$. We assume $\nu_0 = 1\text{ns}^{-1}$ for all of the transitions in Table I, which allows us to determine the temperature dependence of the effective migration rate, but not the absolute value of the rate itself.

The results of our calculation are shown as the black points in Fig. 16(a). The gray line shows the temperature dependence that would be expected had the effective defect migration rate been governed only by the highest activation energy event ($E^{act}_{eff} = 0.4$ eV). The migration rates obtained from kMC dip below this simple prediction at high temperatures, indicating that the multiplicity of transitions occurring in a single migration event reduces the overall point defect migration rate. This reduction may be represented as a temperature-dependent effective attempt frequency.

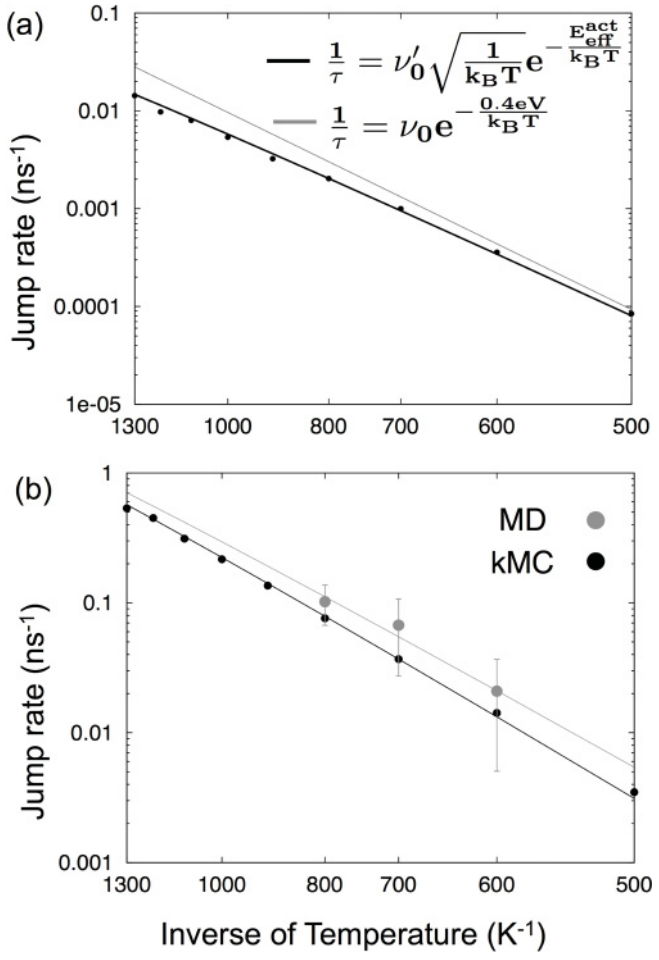

FIG. 16. (a) Comparison between effective defect migration rates computed using kMC (black dots), a standard Arrhenius-type equation using only the highest activation energy event ($E^{act}_{eff} =$ 0.4 eV, gray line), and the modified rate expression in Eq. (8) with a temperature-dependent prefactor (black line). (b) Fits of the modified rate expression to MD data (gray dots). Temperatures are plotted on an inverse scale.

To better understand the origin of this temperature dependence, we revisit harmonic TST.[64] In this formalism, the initial state (A) is separated from the final state by a unique hypersurface (S) and the escape rate Γ is given by

$$\Gamma = \sqrt{\frac{k_B T}{2\pi}} \frac{\int_S e^{-\frac{E_S}{k_B T}} dS}{\int_A e^{-\frac{E_A}{k_B T}} dA}. \tag{2}$$

Here, the numerator is the configurational partition function of the saddle-point hypersurface, while the denominator is the configurational partition function of the hyperspace (A) corresponding to the initial state. For a system with N degrees of freedom, the energy surfaces near the saddle point and initial states may be approximated with Taylor expansions in phase space, parametrized through modal coordinates q_j and q'_j:

$$E_A \approx E(A) + \sum_{j=1}^{N} \frac{1}{2}(2\pi\nu_j)^2 q_j^2, \tag{3}$$

$$E_S \approx E(S) + \sum_{j=1}^{N-1} \frac{1}{2}(2\pi\nu'_j)^2 q_j'^2. \tag{4}$$

ν_j and ν'_j are normal mode vibration frequencies about the initial and the saddle points, respectively. The normal mode perpendicular to the saddle-point hypersurface has an imaginary vibration frequency and is not part of the sum in Eq. (4). Therefore, only $N-1$ degrees of freedom are taken into account when computing the configurational partition function for the saddle point.

When energies are expressed as in Eqs. (3) and (4), the configurational integrals in Eq. (2) become

$$\Gamma = \left(\sqrt{\frac{k_B T}{2\pi}} \frac{\prod_{j=1}^{N-1} \frac{1}{\nu'_j} \sqrt{\frac{k_B T}{2\pi}}}{\prod_{j=1}^{N} \frac{1}{\nu_j} \sqrt{\frac{k_B T}{2\pi}}} \right) \frac{e^{-\frac{E(S)}{k_B T}}}{e^{-\frac{E(A)}{k_B T}}}. \tag{5}$$

The terms in parentheses on the right-hand side of Eq. (5) together form the effective attempt frequency ν_o. Simplifying this expression, the attempt frequency is found to be independent of temperature:

$$\Gamma = \frac{\prod_{j=1}^{N-1} \frac{1}{\nu'_j}}{\prod_{j=1}^{N} \frac{1}{\nu_j}} e^{-\frac{E(S)-E(A)}{k_B T}} = \nu_0 e^{-\frac{E^{act}}{k_B T}}. \tag{6}$$

This expression is only valid if the saddle-point configuration partition function has just one degree of freedom less than the initial state. In some cases, however, there may be additional modes that do not contribute temperature-dependent terms to the configurational partition function, for example, when the saddle point contains rotations or translations not present in the initial state. Büttiker and Christen suggested that in some such cases, the integration across the saddle cannot be treated by a Gaussian approximation, as in the usual case where the saddle has positive curvatures in all directions not along the MEP. Instead, the flatness of a saddle point in one direction can be modeled as a "translational" degree of freedom accessible to the system at the saddle point.[65] A similar interpretation may be applied in this work. Abstracting away from the detailed MEPs illustrated in Fig. 9, all the intermediate states in the

migration process with their multiple minima may be thought of as a single "flat" degree of freedom at the saddle point.[65]

Taking initial and final states corresponding to a defect residing at neighboring MDIs, we attempt to represent all of the intermediate states with a single "effective" saddle point of this kind. To account for the multiple states that comprise the effective saddle point, we consider the saddle point to be a hypersurface with one translational mode. Therefore, the saddle point has $N-2$ vibrational degrees of freedom instead of $N-1$ degrees of freedom as in the case of migration involving a single jump through a unique saddle point. Hence, Eqs. (5) and (6) become

$$\Gamma = \sqrt{\frac{k_B T}{2\pi}} \frac{A_0 \prod_{j=1}^{N-2} \frac{1}{\nu_j'} \sqrt{\frac{k_B T}{2\pi}}}{\prod_{j=1}^{N} \frac{1}{\nu_j} \sqrt{\frac{k_B T}{2\pi}}} \frac{e^{-\frac{E(S)}{k_B T}}}{e^{-\frac{E(A)}{k_B T}}}, \tag{7}$$

$$\Gamma = \sqrt{\frac{2\pi}{k_B T}} \frac{A_0 \prod_{j=1}^{N-2} \frac{1}{\nu_j'}}{\prod_{j=1}^{N} \frac{1}{\nu_j}} e^{-\frac{E(S)-E(A)}{k_B T}} = \nu_0' \frac{1}{\sqrt{k_B T}} e^{-\frac{E^{\mathrm{act}}}{k_B T}}, \tag{8}$$

where A_0 is a constant contributed by the translational mode[65] to the configurational partition function. The attempt frequency predicted by this expression is temperature dependent.

The expression in Eq. (8) is identical to those obtained for models of an overdamped elastic spring on a nonlinear potential surface. Such a spring also has a translational mode and has been used as a model for nucleation and motion of kink pairs on overdamped solitons in spatially one-dimensional systems[65–69] and for nucleation of kink pairs on dislocations in two-dimensional Frankel-Kontorova models.[70] Our kMC results fit very well to Eq. (8) with an effective activation barrier $E_{\mathrm{eff}}^{\mathrm{act}} = 0.398 \pm 0.002$ eV, as illustrated by the black line in Fig. 16(a).

The numerical value of the ν_0' may be determined directly from MD simulations by counting the number of times a defect jumps from one MDI to another in a fixed time interval. We assumed that point defect migration follows a Poisson process[71] in which the probability that exactly s events occur in a time interval t is given by

$$p(t/\tau, s) = \frac{(t/\tau)^s e^{-t/\tau}}{s!}. \tag{9}$$

Here, $\tau = \frac{1}{\Gamma}$ is the average waiting time for a defect to migrate to an adjacent MDI. We performed $N_0 = 64$ independent MD runs of a vacancy at an MDI in the Cu-Nb interface. These runs were repeated at three different temperatures: $T \in \{600, 700, 800\}$ K. The duration of each run was 8.11 ns (t_{tot}). In each run, migration events were identified by direct inspection of atomic configurations recorded at intervals of 40.5 ps. From the investigation described in Sec. III C1, we know that the typical duration of a complete migration event at $T = 800$ K is 32.5 ps. Thus, the selected time interval between consecutive recordings minimizes the total number of configurations that must be saved and analyzed while ensuring that no more than one migration event occurs between recordings. While no migration events were observed in some runs, as many as three distinct ones were observed in others. For a given temperature, we identify the probability $p(t_{\mathrm{tot}}/\tau, s) = \frac{n(s)}{N_0}$ that the point defect migrated to an adjacent MDI exactly s times, where $n(s)$ is the number of runs in which exactly s migration events occurred and plotted in Fig. 17 as histograms. We use these probabilities to determine τ from a least-squares fit in s to

$$\ln[(s!)p(t/\tau, s)] = s \ln(t/\tau) - t/\tau. \tag{10}$$

Good fits are obtained for all three temperatures, confirming our assumption that point defect migration follows a Poisson process (Fig. 17). The jump rates for each temperature, obtained by fitting, are plotted in Fig. 16(b) as filled gray circles with uncertainties corresponding to the error in the least-squares fit. The gray line is the least-squares fit of Eq. (8) to the rates obtained from MD. The activation energy obtained from our kMC model ($E_{\mathrm{eff}}^{\mathrm{act}} = 0.398 \pm 0.002$ eV) is well within the uncertainty of the activation energy found by fitting the MD data, namely, $E_{\mathrm{eff}}^{\mathrm{act}} = 0.374 \pm 0.045$ eV.

The effective attempt frequency for defect migration obtained by fitting the MD data is $\nu_0' = 6.658 \times 10^9 \pm 2.7 \times 10^6$ s^{-1}. This value is several orders of magnitude lower than typical attempt frequencies for point defect migration in fcc Cu, namely, $10^{12}-10^{14}$ s^{-1}.[72–74] A mechanistic interpretation for such a low migration attempt frequency is not immediately forthcoming. One possible explanation is that it arises from the large number of atoms participating in the migration process. The attempt frequency for migration of compact point defects might be expected to be on the order of the Einstein frequency because it involves the motion of only one atom. However, the migration mechanism discussed here involves collective motion of many atoms. Their collective oscillation in a vibrational mode that leads up to the saddle point for defect migration may have a considerably lower frequency

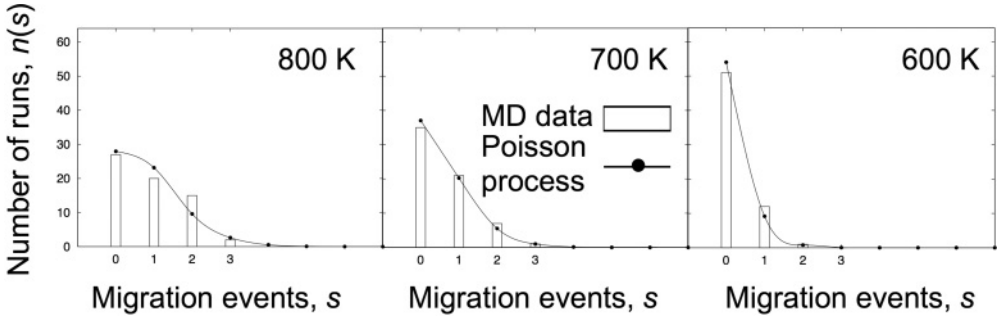

FIG. 17. Comparison between the MD data (histograms) to the fits obtained by assuming that point defect migration follows a Poisson process (continuous curves and data points).

than an Einstein oscillator. This interpretation, however, is at odds with other collective processes, such as the spontaneous transformation of small voids to stacking fault tetrahedra, the effective attempt frequency of which is several orders of magnitude higher than the Einstein frequency.[75]

Delocalized point defect migration from one MDI to another may also involve passage through several intermediate metastable states that do not assist migration: the $\mathbf{I}'$ states described in Sec. III C1. Therefore, the defect is likely to spend more time between the initial and final states than it would had there been only one saddle point, lowering the effective attempt frequency. If this were to completely account for the lowering of the attempt frequency, however, then nucleation of $\mathbf{I}'$ states would have to occur several orders of magnitude more frequently than the completion of a migration step, which is not what we observe. Finally, conventional transition-state theory overestimates attempt frequencies by assuming that every time a point defect crosses the saddle point, it reaches the final state. In reality, however, a saddle point may be recrossed several times before reaching the final state,[76] reducing the value of the pre-factor as derived by transition-state theory.[64] Further work is needed to determine which, if any, of these explanations is the correct one.

IV. DISCUSSION

We have shown that the migration of delocalized vacancies and interstitials at a Cu-Nb interface is governed by a finite set of definite mechanisms that are directly related to the structure of the interface misfit dislocation network. Our simulations further show that the mechanisms of point defect cluster formation, migration, and dissociation have several commonalities with those of isolated point defect migration. In both cases, activation energies are governed by the formation of thermal kink pairs. We therefore conclude that vacancies and interstitials at the Cu-Nb interface we studied may be viewed as genuine point defects, even though they are delocalized. Furthermore, on the basis of this description, we formulated analytical models for the temperature dependence of defect migration rates. Previous work has also shown that complete minimum energy defect migration paths may be calculated analytically based on this description using dislocation mechanics.[40]

Previous atomistic modeling studies conducted at other interfaces where point defects may delocalize found that diffusion could occur either through single-atom jumps or through collective displacements of lines of atoms with activation energies that ranged from 0.3 to 1.0 eV.[12,14,77–80] By contrast to the work reported here, these studies cataloged numerous diffusion paths, but did not identify common structural features among them nor did they propose models that could relate diffusion to the underlying structure of the defect-free interfaces. It was therefore not clear from them whether the diffusion mechanisms they identified could be usefully described using a framework centered on the "defect" concept.

Wang and co-workers[81] indirectly addressed the question of point defect diffusion at Cu-Nb interfaces in a modeling study that demonstrated room-temperature climb of dislocations in Cu-Nb interfaces. The migration energies they reported were about a factor of 4 lower than those described here. The apparent discrepancy between their study and ours is likely due to the fact that the full point defect migration mechanism was not identified in that study. The energy barrier calculated in it compares well with barriers for transitions of the type $\mathbf{I} \rightarrow \mathbf{t} \rightarrow \mathbf{B}$ or $\mathbf{B} \rightarrow \mathbf{t} \rightarrow \mathbf{I}'$, shown in Fig. 8(c). Moreover, since the formation of thermal kink pairs is sensitive to the internal stresses, introduction of extrinsic dislocations into the Cu-Nb interface may alter the point defect migration mechanism itself.

Our study suggests that vacancies and interstitials may not readily form clusters at the Cu-Nb interface. Instead, they are likely to remain isolated at nonzero temperature. This behavior may be beneficial under conditions where numerous point defects are created, for instance, under irradiation, because it may reduce the tendency to form voids or precipitates. Interfaces with such properties may therefore absorb defects created in the neighboring layers without becoming damaged themselves. Indeed, interfaces are thought to be responsible for the enhanced radiation damage resistance of Cu-Nb multilayer nanocomposites.[13,82] They are also thought to delay precipitation of implanted He into nanoscale bubbles.[83–85] Similar behaviors have also been observed in other heterophase interfaces such as Ag-V,[86] Cu-V,[87] and Cu-Mo,[88] suggesting that these interfaces may have similar defect clustering properties as Cu-Nb.

In many cases, the time scales accessible to conventional MD methods are too small to study defect migration. They are sufficient in the Cu-Nb interface we studied due to a confluence of several factors. Defect trapping sites (MDIs) were spaced closely enough for the thermal-kink-pair nucleation mechanism to obviate the need for defects to detrap from MDIs before they could migrate. Thermal-kink nucleation energies were small and their effective attempt frequencies high. However, there may be other interfaces with misfit dislocation intersections far enough, migration barriers high enough, or attempt frequencies low enough that it may not be possible to model vacancy and interstitial migration using conventional MD.

For example, in Cu-V interfaces, point defects delocalize to form kink-jog pairs at MDIs, just as in Cu-Nb.[56] However, the distance between MDIs along misfit dislocations in Cu-V interfaces is about 70 Å.[56] Thermal kink pairs forming at these MDIs are therefore not likely to aid migration as they cannot extend sufficiently far to interact with delocalized defects at neighboring MDIs. Nonetheless, it may be possible to make quantitative predictions for defect migration processes at such interfaces by extending the dislocation-based model developed on the basis of the work described in Ref. 40. It may also be possible to incorporate such descriptions of defect migration mechanisms into dislocation dynamics[89,90] or phase field models.[91]

Atomistic simulation techniques that artificially accelerate thermally activated processes may help to identify migration mechanisms at interfaces where conventional MD time scales are too small. Examples of such methods are temperature accelerated dynamics (TAD),[92] the parallel-replica method,[93] activation-relaxation techniques (ART),[94,95] and variants of algorithms where energy basins are filled by introducing artificial potentials, some of which are called metadynamics[96,97] and other hyperdynamics.[98,99]

In practice, however, applying such techniques may not be straightforward. For example, methods such as TAD may fail if the mechanisms operative at high temperatures are not the same as those relevant at lower ones, which may be the case if different structural phases are stable at these two different temperatures. Both TAD and the parallel-replica method are most efficient when used on transitions governed by high activation energies. Their efficiency, however, is very poor for systems such as the interface we studied, which has a rough potential energy landscape with numerous shallow metastable minima separated by a continuous distribution of small energy barriers. Automatic event-determining and barrier-hopping techniques such as metadynamics, hyperdynamics, and ART are also limited by this so-called "small-barrier problem."[100]

One way in which the small-barrier problem might be circumvented is if improved criteria for identifying events become available. Conventional event detection relies on computationally intensive schemes, such as periodic comparisons of inherent structures obtained from energy minimization, or simple metrics such as the distance moved by an atom or a certain number of atoms. Criteria more sensitive to the actual structure of the transitions under investigation, such as the fivefold ring detection algorithm used in this study, may improve the efficiency of accelerated MD methods by helping to ignore "irrelevant" transitions that do not contribute to the phenomenon of interest. It may, however, be difficult to develop such criteria without prior knowledge of the operative mechanisms. Furthermore, in some cases, the influence of the ignored irrelevant transitions may not be immediately obvious. In our study, the role of the multiple states involved in delocalized point defect migration is only to give rise to an effective migration rate with a lower magnitude and different temperature dependence than in events with a single activation energy barrier.

The most likely methods for experimentally validating the defect migration mechanisms found in this study do not rely on direct observation. In particular, since point defect migration occurs preferentially along one of the misfit dislocation lines, diffusivities along this interface may be expected to be highly anisotropic, an experimentally testable prediction. The numerical values of such experimentally determined diffusivities may be expected to reflect the temperature-dependent prefactor and low effective attempt frequency ν_0' predicted in Sec. III D. Additionally, because the defect migration mechanisms described here depend on the motion of kinks and jogs, they are likely to be sensitive to externally applied stresses that result in Peach-Koehler forces[55] acting on these kinks and jogs. Resolved stresses that oppose thermal-kink-pair nucleation may raise migration energy barriers, while opposite ones would reduce them. Direct observation of the mechanisms governing point defect migration at this or any other interface is not currently possible due to inadequate spatial and temporal resolution of available experimental tools. Continued development of multi-length- and time-scale characterization methods may nevertheless one day enable such observations.[101]

V. CONCLUSIONS

We have demonstrated that delocalized vacancies and interstitials at semicoherent Cu-Nb interfaces have clearly discernible structures and exhibit definite migration and clustering mechanisms. Nucleation of thermal kink pairs plays a central role in all of these mechanisms. The migration of the delocalized vacancies and interstitials is a multistep process involving several metastable states. A consequence of these multiple stages is that the prefactor of the Arrhenius-type rate expression is dependent on temperature. Finally, the structure and migration of delocalized vacancies, interstitials, and clusters thereof may be described using dislocation-based models, thereby directly relating defect migration to interface structure. Thus, vacancies and interstitials at Cu-Nb interfaces may be viewed as genuine defects, albeit governed by mechanisms of higher complexity than conventional point defects in crystalline solids.

ACKNOWLEDGMENTS

We thank A. Misra, J. P. Hirth, R. G. Hoagland, J. Wang, I. J. Beyerlein, B. Uberuaga, and X.-Y. Liu for fruitful discussions. K.K. thanks M. Kabir for many fruitful discussions. This research was funded by the US Department of Energy, Office of Science, Office of Basic Energy Sciences under Award No. 2008LANL1026 through the *Center for Materials at Irradiation and Mechanical Extremes*, an Energy Frontier Research Center at Los Alamos National Laboratory. Computing resources used for migration rate simulations were provided by the Extreme Science and Engineering Discovery Environment (XSEDE), supported by the National Science Foundation under Grant No. OCI-1053575.

*kkolluri@lanl.gov

[1] P. G. Shewman, *Diffusion in Solids*, 2nd ed. (Wiley, New York, 1989).
[2] D. J. Bacon and Y. N. Osetsky, Int. Mater. Rev. **47**, 233 (2002).
[3] A. S. Argon, *Strengthening Mechanisms in Crystal Plasticity* (Oxford University Press, Oxford, UK, 2008).
[4] L. K. Mansur, Nucl. Technol. **40**, 5 (1978).
[5] V. Fidleris, At. Energy Rev. **13**, 51 (1975).
[6] W. Jaeger and H. Gleiter, Scr. Metall. **12**, 675 (1978).
[7] P. A. Thorsen, B. J. Bilde-Sørensen, and B. N. Singh, Materials Science Forum **207**, 445 (1996).
[8] M. J. Demkowicz, O. Anderoglu, X. Zhang, and A. Misra, J. Mater. Res. **26**, 1666 (2011).
[9] A. Brokman, P. D. Bristowe, and R. W. Balluffi, J. Appl. Phys. **52**, 6116 (1981).
[10] W. Hahn and H. Gleiter, Acta Metall. **29**, 601 (1981).
[11] H. Gleiter, Mater. Sci. Eng. **52**, 91 (1982).
[12] A. Suzuki and Y. Mishin, Interface Sci. **11**, 131 (2003).
[13] M. J. Demkowicz, R. G. Hoagland, and J. P. Hirth, Phys. Rev. Lett. **100**, 136102 (2008).
[14] M. R. Sørensen, Y. Mishin, and A. F. Voter, Phys. Rev. B **62**, 3658 (2000).

[15]T. E. Mitchell, Y. C. Lu, A. J. Griffin Jr., M. Nastasi, and H. Kung, J. Am. Ceram. Soc. **80**, 1673 (1997).
[16]M. J. Demkowicz, J. Wang, and R. G. Hoagland, in *Dislocations in Solids*, edited by J. P. Hirth, Chap. 83, Vol. 14 (Elsevier, Amsterdam, 2007), pp. 141–206.
[17]I. Kaur, Y. Mishin, and W. Gust, *Fundamentals of Grain and Interphase Boundary Diffusion*, 3rd ed. (Wiley, New York, 1995).
[18]A. P. Sutton and R. W. Balluffi, *Interfaces in Crystalline Materials* (Oxford University Press, Oxford, UK, 1995).
[19]R. E. Hoffman and D. Turnbull, J. Appl. Phys. **22**, 634 (1951).
[20]J. C. M. Hwang, J. D. Pan, and R. W. Balluffi, J. Appl. Phys. **50**, 1349 (1979).
[21]S. R. L. Couling and R. Smoluchowski, J. Appl. Phys. **25**, 1538 (1954).
[22]R. W. Balluffi, A. Brokman, and A. H. King, Acta Metall. **30**, 1453 (1982).
[23]J. P. Hirth and R. C. Pond, Acta Mater. **44**, 4749 (1996).
[24]R. C. Hugo and R. G. Hoagland, Acta Mater. **48**, 1949 (2000).
[25]D. Turnbull and R. E. Hoffman, Acta Metall. **2**, 419 (1954).
[26]J. Sommer, C. Herzig, S. Mayer, and W. Gust, Defect Diffusion Forum **66–69**, 843 (1989).
[27]A. Suzuki and Y. Mishin, Interface Sci. **11**, 425 (2003).
[28]R. Smoluchowski, in *Defects in Crystalline Solids* (Physical Society, Great Britain, 1955), p. 197.
[29]T. Kwok, P. S. Ho, and S. Yip, Phys. Rev. B **29**, 5354 (1984).
[30]M. Nomura and J. B. Adams, J. Mater. Res. **10**, 2916 (1995).
[31]V. Vitek, A. P. Sutton, G. J. Wang, and D. Schwartz, Scr. Metall. **17**, 183 (1983).
[32]V. Vitek, Y. Minonishi, and G.-J. Wang, J. Phys. Colloques **46**, 171 (1985).
[33]A. Suzuki and Y. Mishin, J. Mater. Sci. **40**, 3155 (2005).
[34]T. Kwok, P. S. Ho, S. Yip, R. W. Balluffi, P. D. Bristowe, and A. Brokman, Phys. Rev. Lett. **47**, 1148 (1981).
[35]T. Kwok, P. S. Ho, and S. Yip, Phys. Rev. B **29**, 5363 (1984).
[36]F. Gao, H. L. Heinisch, and R. J. Kurtz, J. Nucl. Mater. **386**, 390 (2009).
[37]A. H. King and D. A. Smith, Philos. Mag. A **42**, 495 (1980).
[38]B. N. Singh, T. Leffers, W. V. Green, and M. Victoria, J. Nucl. Mater. **125**, 287 (1984).
[39]P. L. Lane and P. J. Goodhew, Philos. Mag. A **48**, 965 (1983).
[40]K. Kolluri and M. J. Demkowicz, Phys. Rev. B **82**, 193404 (2010).
[41]S. M. Foiles, M. I. Baskes, and M. S. Daw, Phys. Rev. B **33**, 7983 (1986).
[42]M. S. Daw, S. M. Foiles, and M. I. Baskes, Mater. Sci. Rep. **9**, 251 (1993).
[43]M. J. Demkowicz and R. G. Hoagland, Int. J. Appl. Mech. **1**, 421 (2009).
[44]J. Wang, R. G. Hoagland, X.-Y. Liu, and A. Misra, Acta Mater. **59**, 3164 (2011).
[45]J. Wang and A. Misra, Curr. Opin. Solid State Mater. Sci. **15**, 20 (2011).
[46]M. Demkowicz and L. Thilly, Acta Mater. **59**, 7744 (2011).
[47]A. Leach, *Molecular Modelling: Principles and Applications*, 2nd ed. (Prentice Hall, Englewood Cliffs, NJ, 2001).
[48]S. Plimpton, J. Comput. Phys. **117**, 1 (1995).
[49]M. Parrinello and A. Rahman, J. Appl. Phys. **52**, 7182 (1981).
[50]J. Wang, R. G. Hoagland, J. Hirth, and A. Misra, Acta Mater. **56**, 5685 (2008).
[51]T. Schneider and E. Stoll, Phys. Rev. B **17**, 1302 (1978).
[52]G. Henkelman, B. P. Uberuaga, and H. Jonsson, J. Chem. Phys. **113**, 9901 (2000).
[53]G. Henkelman and H. Jonsson, J. Chem. Phys. **113**, 9978 (2000).
[54]J. Li, Modell. Simul. Mater. Sci. Eng. **11**, 173 (2003).
[55]J. P. Hirth and J. Lothe, *Theory of Dislocations*, 2nd ed. (Krieger, Malabar, Florida, 1992).
[56]M. J. Demkowicz, D. Bhattacharyya, I. Usov, Y. Q. Wang, M. Nastasi, and A. Misra, Appl. Phys. Lett. **97**, 161903 (2010).
[57]R. A. Johnson, Phys. Rev. **152**, 629 (1966).
[58]Y. N. Osetsky, M. Victoria, A. Serra, S. I. Golubov, and V. Priego, J. Nucl. Mater. **251**, 34 (1997).
[59]Yu. N. Osetsky, A. Serra, B. N. Singh, and S. I. Golubov, Philos. Mag. A **80**, 2131 (2000).
[60]G. Simmons and H. Wang, *Single Crystal Elastic Constants and Calculated Aggregate Properties: A Handbook*, 2nd ed. (MIT Press, Cambridge, Massachusetts, 1971).
[61]T. Vegge, J. P. Sethna, S.-A. Cheong, K. W. Jacobsen, C. R. Myers, and D. C. Ralph, Phys. Rev. Lett. **86**, 1546 (2001).
[62]T. Vegge, T. Leffers, O. Pedersen, and K. Jacobsen, Mater. Sci. Eng. A **319–321**, 119 (2001).
[63]A. B. Bortz, M. H. Kalos, and J. L. Lebowitz, J. Comput. Phys. **17**, 10 (1975).
[64]G. H. Vineyard, J. Phys. Chem. Solids **3**, 121 (1957).
[65]M. Büttiker and T. Christen, Phys. Rev. Lett. **75**, 1895 (1995).
[66]V. Celli, M. Kabler, T. Ninomiya, and R. Thomson, Phys. Rev. **131**, 58 (1963).
[67]M. Büttiker and R. Landauer, Phys. Rev. Lett. **43**, 1453 (1979).
[68]J. F. Currie, J. A. Krumhansl, A. R. Bishop, and S. E. Trullinger, Phys. Rev. B **22**, 477 (1980).
[69]M. Büttiker and R. Landauer, Phys. Rev. A **23**, 1397 (1981).
[70]D. Rodney and L. Proville, Phys. Rev. B **78**, 104115 (2008).
[71]G. F. Lawler, *Introduction to Stochastic Processes*, 2nd ed. (Chapman and Hall/CRC, New York, 2006).
[72]H. Mehrer and A. Seeger, Phys. Status Solidi B **35**, 313 (1969).
[73]M. J. Sabochick and S. Yip, J. Phys. F: Met. Phys. **18**, 1689 (1988).
[74]Y. Mishin, M. J. Mehl, D. A. Papaconstantopoulos, A. F. Voter, and J. D. Kress, Phys. Rev. B **63**, 224106 (2001).
[75]B. P. Uberuaga, R. G. Hoagland, A. F. Voter, and S. M. Valone, Phys. Rev. Lett. **99**, 135501 (2007).
[76]P. Hänggi and M. Borkovec, Rev. Mod. Phys. **62**, 251 (1990).
[77]Q. Ma, C. L. Liu, J. B. Adams, and R. W. Balluffi, Acta Metall. Mater. **41**, 143 (1993).
[78]P. Keblinski, D. Wolf, and H. Gleiter, Interface Sci. **6**, 205 (1998).
[79]V. Yamakov, D. Wolf, S. R. Phillpot, and H. Gleiter, Acta Mater. **50**, 61 (2002).
[80]T. Frolov and Y. Mishin, Phys. Rev. B **79**, 174110 (2009).
[81]J. Wang, R. G. Hoagland, and A. Misra, Appl. Phys. Lett. **94**, 131910 (2009).
[82]A. Misra, M. J. Demkowicz, X. Zhang, and R. G. Hoagland, J. Mater. **59**, 62 (2007).
[83]T. Höchbauer, A. Misra, K. Hattar, and R. G. Hoagland, J. Appl. Phys. **98**, 123516 (2005).
[84]X. Zhang, N. Li, O. Anderoglu, H. Wang, J. G. Swadener, T. Höchbauer, A. Misra, and R. G. Hoagland, Nucl. Instrum. Methods Phys. Res., Sect. B **261**, 1129 (2007).
[85]K. Hattar, M. Demkowicz, A. Misra, I. Robertson, and R. Hoagland, Scr. Mater. **58**, 541 (2008).
[86]Q. Wei, Y. Wang, M. Nastasi, and A. Misra, Philos. Mag. **91**, 553 (2011).

[87]E. G. Fu, A. Misra, H. Wang, L. Shao, and X. Zhang, J. Nucl. Mater. **407**, 178 (2010).
[88]N. Li, J. J. Carter, A. Misra, L. Shao, H. Wang, and X. Zhang, Philos. Mag. Lett. **91**, 18 (2011).
[89]B. Devincre and L. P. Kubin, Modell. Simul. Mater. Sci. Eng. **2**, 559 (1994).
[90]K. W. Schwarz, J. Appl. Phys. **85**, 108 (1999).
[91]Y. Wang and J. Li, Acta Mater. **58**, 1212 (2010).
[92]M. R. Sørensen and A. F. Voter, J. Chem. Phys. **112**, 9599 (2000).
[93]A. F. Voter, Phys. Rev. B **57**, R13985 (1998).
[94]R. Malek and N. Mousseau, Phys. Rev. E **62**, 7723 (2000).
[95]E. Machado-Charry, L. K. Béland, D. Caliste, L. Genovese, T. Deutsch, N. Mousseau, and P. Pochet, J. Chem. Phys. **135**, 034102 (2011).
[96]A. Kushima, X. Lin, J. Li, J. Eapen, J. C. Mauro, X. Qian, P. Diep, and S. Yip, J. Chem. Phys. **130**, 224504 (2009).
[97]A. Laio and M. Parrinello, Proc. Natl. Acad. Sci. USA **99**, 12562 (2002).
[98]A. F. Voter, Phys. Rev. Lett. **78**, 3908 (1997).
[99]R. A. Miron and K. A. Fichthorn, J. Chem. Phys. **119**, 6210 (2003).
[100]R. A. Miron and K. A. Fichthorn, Phys. Rev. Lett. **93**, 128301 (2004).
[101]I. M. Robertson, C. A. Schuh, J. S. Vetrano, N. D. Browning, D. P. Field, D. J. Jensen, M. K. Miller, I. Baker, D. C. Dunand, R. Dunin-Borkowski, B. Kabius, T. Kelly, S. Lozano-Perez, A. Misra, G. S. Rohrer, A. D. Rollett, M. L. Taheri, G. B. Thompson, M. Uchic, X.-L. Wang, and G. Was, J. Mater. Res. **26**, 1341 (2011).